Materials Science in Semiconductor Processing 206 (2026) 110460

Contents lists available at ScienceDirect

Materials Science in Semiconductor Processing

journal homepage: www.elsevier.com/locate/mssp

Regulating the H_2 selectivity of MoS_2 sensors through synergistic metal–non-metal co-doping

Zuxun Zhang, Lin Tao *, Xin Quan, Mingyang Gu, Han Zhang, Baigang An, Lixiang Li **

School of Chemical Engineering, University of Science and Technology Liaoning, Anshan, 114051, China

ARTICLE INFO

Keywords:
MoS_2 monolayer
H_2 sensing
Electrical response
Transition metal decorated
Density functional theory

ABSTRACT

The selective detection of hydrogen (H_2) in complex gas environments is essential for hydrogen safety monitoring, yet remains challenging for pristine MoS_2-based sensors. Herein, density functional theory (DFT) was employed to explore four single-layer MoS_2 systems co-doped with either Sc or Ti (metal site) and B or N (non-metal site), namely Sc@B-MoS_2, Sc@N-MoS_2, Ti@B-MoS_2, and Ti@N-MoS_2. Formation energy analysis (−3.34 to −3.01 eV) confirmed their structural stability. Adsorption energy results reveal that Sc@N-MoS_2 (−0.35 eV) and Ti@N-MoS_2 (−0.31 eV) exhibit the most favorable H_2 binding, markedly outperforming single-atom doping. The d-band center analysis and density of states (DOS) calculations show that N-site modification enhances orbital overlap with H_2, preserving high H_2 selectivity even in the presence of CO and H_2O. The Crystal Orbital Hamilton Population (COHP) analysis indicates that bonding states below the Fermi level dominate during adsorption, enabling strong gas-surface interactions. Gibbs free energy calculations suggest robust thermal stability up to 500 K, while diffusion barriers of 3.46–3.86 kJ/mol indicate the high mobility of adsorbed molecules, contributing to rapid sensor response kinetics. By calculating the electrical response and recovery time, we demonstrated that this material exhibits a shorter recovery time and high electrical responsiveness. Overall, Sc@N-MoS_2 demonstrated superior sensing performance, providing mechanistic insights and design principles for synergistically co-doped MoS_2 sensors with high H_2 selectivity under realistic conditions.

1. Introduction

Hydrogen has emerged as a promising clean energy alternative to fossil fuels, owing to its superior mass energy density and the characteristic of generating only water upon combustion [1–3]. However, owing to the extremely low ignition threshold and nanoscale molecular dynamics diameter of hydrogen, it has significant flammability and diffusion characteristics, posing a major explosion hazard in industrial, transportation, and storage environments [4,5]. Thus, the rapid, selective, and stable detection of hydrogen is essential for ensuring operational safety in the hydrogen energy industry.

In gas-sensing technology, the structural characteristics and surface chemical behavior of gas-sensitive materials directly determine the core performance of the sensor [6,7]. Two-dimensional materials have opened up novel breakthrough avenues for gas sensing technology, thanks to their distinctive layered structure and superior electrical properties [8]. Of these materials, molybdenum disulfide (MoS_2) stands as a typical example of transition metal dichalcogenides (TMDs), with considerable promise for gas-sensing uses due to its adjustable bandgap structure, ample surface active sites, and superior chemical stability [9,10]. However, intrinsic MoS_2 suffers from inherent drawbacks, such as surface inertness, insufficient electrical response, and weak gas molecule adsorption capacity, which severely limit its sensing performance. Research indicates that First-principles calculations have revealed that small molecular gases, including H_2, O_2, and CO, exhibit only weak physical adsorption on MoS_2 surfaces. Their charge transfer is negligible, and their impact on the band structure of the material is minimal [11]. To overcome this technical bottleneck, researchers have innovatively adopted an atomic-level doping strategy, precisely controlling the band structure and surface active site distribution of MoS_2 to significantly enhance the sensing properties of the material [12].

In the field of advanced gas-sensitive materials research, the utilization of transition metal elements to modulate the properties of MoS_2-based materials has emerged as a prominent research focus in recent years. Early studies [13] demonstrated that Ir element modification significantly enhances the MoS_2 adsorption capacity for gases such as

* Corresponding author. School of Chemical Engineering, University of Science and Technology Liaoning, Anshan, 114051, China.
** Corresponding author. School of Chemical Engineering, University of Science and Technology Liaoning, Anshan, 114051, China.
E-mail addresses: taolin@ustl.edu.cn (L. Tao), lxli2005@126.com (L. Li).

https://doi.org/10.1016/j.mssp.2026.110460
Received 9 September 2025; Received in revised form 7 January 2026; Accepted 20 January 2026
Available online 24 January 2026

CH_4, C_2H_4, and C_2H_2, providing a crucial direction for research on the transition-metal-regulated gas-sensing performance of MoS_2. Building on this concept, subsequent computational studies [14] confirmed that modifying MoS_2 with Ni and Pt not only retains the advantage of enhancing the gas adsorption capacity, but also significantly improves its sensing performance for gases such as CO and NO.

As research continues to advance, the academic community has begun to focus on the impact of transition metal modifications on the adsorption properties of specific gases such as H_2. It can be found that MoS_2 modified with Y or Ti can significantly enhance the adsorption energy of H_2 molecules, further validating the importance of transition metals in regulating the properties of MoS_2-based materials [15,16]. Additionally, the hydrogen adsorption effects of nine transition metals-including Fe, Co, and Ni-doped into MoS_2, revealing that the Os-doped system exhibited the strongest H_2 adsorption capacity, with an adsorption energy as high as 1.10 eV [17]. Interestingly, platinum-modified MoS_2 possesses unique advantages, simultaneously enhancing both the intrinsic electrical response of MoS_2 and its adsorption performance for multiple gases, offering new insights for developing multi-gas synergistic detection technologies [18].

However, this also highlights certain limitations of transition metal doping, such as [18,19] wherein metal atoms indiscriminately enhance the adsorption of multiple gases. This directly diminishes the material's ability to recognize target gases, hindering precise detection of specific gases. On the other hand, under long-term operating conditions, metal nanoparticles are prone to agglomeration, compromising the structural stability of the material [20]. These issues significantly limit the practical applicability of transition metal-doped MoS_2 materials.

Therefore, numerous researchers have turned to non-metallic doping of MoS_2 to enhance the selectivity of materials toward specific gases. For instance, introducing Si into the S sites of MoS_2 significantly improved the material's adsorption performance for H_2 [21]. Surprisingly, when MoS_2 was doped with B and C, it specifically enhanced the chemical adsorption of N_2 while maintaining weak physical adsorption of CH_4 [22]. This discovery offers new insights into the selective adsorption of specific gases. Unfortunately, the low doping efficiency and limited charge transfer capacity of non-metallic doping hinder further improvements in the sensitivity.

It is noteworthy that metal and non-metal doping have been proven to be two effective yet distinct strategies for regulating the gas-sensing performance of MoS_2. Metal doping tends to act as a charge transfer amplifier, directly modulating the electronic structure of the substrate through its d-orbital characteristics. In contrast, non-metal doping focuses more on active site engineering, influencing gas adsorption by altering the surface chemical composition and local coordination environments [23–27]. Existing research demonstrates that co-doping strategies, including bimetallic, bimetallic-nonmetallic, or metal-defect synergies can yield multiple synergistic advantages. These encompass bandgap narrowing, enhanced intrinsic electrical response, and the creation of abundant active sites through induced lattice distortion, defect formation, and phase transition. Furthermore, such strategies contribute to improved durability in harsh environments via structural stabilization and electronic modulation [14,18,28,29]. However, current studies are predominantly focused on electrocatalytic hydrogen evolution reactions (HER), where the core aim is to optimize hydrogen adsorption/desorption kinetics. In contrast, for gas-sensing applications that demand high selectivity, sensitivity, and rapid recovery through the specific and reversible adsorption of target gases the systematic design principles and underlying mechanisms remain largely unexplored. In particular, the deliberate use of synergistic effects between metal and nonmetal dopants to tailor the surface chemistry and electronic structure of MoS_2 for high-performance gas sensing lacks comprehensive theoretical and experimental investigation. It is this critical gap that the present work aims to address.

Employing density functional theory, this work systematically examined the differential adsorption behaviors of H_2, CO, and H_2O on Sc/Ti-B/N co-doped MoS_2. First, four doped monolayer models (Sc@B-MoS_2, Sc@N-MoS_2, Ti@B-MoS_2, and Ti@N-MoS_2) were constructed, and the structural stabilities of these models were confirmed from multiple perspectives. Second, the adsorption properties exhibited by the three gases on distinct single-layer materials, and the microscopic causes of the adsorption differences were explained using d-band center theory. The role of bonding orbitals during gas adsorption was investigated using the Crystal Orbital Hamiltonian Population (COHP). Subsequently, the electrochemical responses of the different monolayers to the three gases were studied by analyzing the density of states (DOS). Finally, Gibbs free energy calculations and kinetic analyses of response recovery were employed to further validate the applicability of the studied materials at actual operating temperatures. This study not only reveals the synergistic mechanisms of metal-nonmetal co-doping at the atomic scale but also provides a critical theoretical foundation and technical roadmap for designing next-generation high-performance hydrogen sensors.

2. Calculation method

2.1. Algorithm settings

Using density functional theory and the Dmol3 module [30], we systematically studied the different behaviors of the Sc@B-MoS_2, Sc@N-MoS_2, Ti@B-MoS_2, and Ti@N-MoS_2 surfaces in capturing H_2, CO, and H_2O. All calculations were spin-polarized to properly account for the electronic structures of systems containing transition metal atoms (Sc and Ti). We adopted the generalized gradient approximation (GGA) with the PBE functional to handle exchange-correlation effects in calculations, and selected a double numerical basis set (DNP) [31,32] that includes a polarization function. For precise characterization of intermolecular weak interactions, all calculations incorporated Grimme's van der Waals correction (DFT-D) [33]. To address the issue of incomplete convergence of interlayer interactions during gas adsorption, we adopted the method proposed by Bal et al. [34]. A real-space cutoff radius of 4.9 Å was employed to control the spatial dispersion of the basis functions. To ensure that the computational model accurately simulates isolated doping and adsorption systems while avoiding interactions between periodic mirror images, rigorous convergence tests were conducted on the supercell dimensions. Ultimately, a $4 \times 4 \times 1$ Monkhorst–Pack grid was selected for Brillouin zone integration to guarantee precise sampling. To ensure computational accuracy, strict convergence criteria were set: a total energy change threshold of 1.0×10^{-5} Ha, an atomic force convergence threshold set to 0.002 Ha/Å, and an atomic displacement threshold of 0.005 Å. Finally, the electronic distribution and charge transfer mechanism of the adsorption system were investigated using Mulliken population analysis [35,36].

2.2. Gas-phase environment model and simplification basis

This study selected two typical interfering gases, CO and water vapor, for investigation for the following reasons: CO, a common reducing gas, exhibits adsorption and charge transfer mechanisms similar to those of H_2, making it an ideal candidate for evaluating H_2 detection selectivity. Second, H_2O represents ubiquitous humidity interference, and assessing moisture resistance is crucial for practical applications. The investigation of these two molecules effectively validated the fundamental principle of distinguishing H_2 from major interferents using the Sc/Ti-B/N co-doping strategy. Crucially, as the first fundamental theoretical study revealing the microscopic mechanism of H_2 sensing in the Sc/Ti-B/N co-doped system, a relatively simplified model is required to elucidate its core mechanism, that is, how metal-nonmetal synergistic interactions specifically enhance H_2 adsorption. Therefore, it is particularly important to avoid introducing gases that would complicate the system or involve competitive adsorption/reaction pathways, such as oxidation and carbonization.

3. Results and discussion

3.1. Structural stability

This study aims to reveal the synergistic regulation mechanism of metal-nonmetal co-doping on the gas-sensing performance of MoS_2. To this end, we constructed intrinsic and Sc/Ti-B/N co-doped MoS_2 models and systematically investigated the adsorption behaviors of H_2, CO, and H_2O molecules. The co-doped models employed the most representative and experimentally feasible two-site substitution configuration: one transition metal atom (Sc/Ti) replaces the Mo site, while one non-metal atom (B/N) replaces its nearest-neighbor S site. This design enables a tight coupling between the two dopants, maximizing the electronic synergistic effects and precisely revealing the core "metal-nonmetal synergy" mechanism. Second, lattice site substitution is thermodynamically more stable and directly corresponds to established experimental pathways for metallic doping at Mo sites and non-metallic doping at S sites. This ensures that the theoretical predictions provide direct guidance for experimental work.

Based on this, we systematically investigated four co-doped systems: Sc@B-, Sc@N-, Ti@B-, and Ti@N-MoS_2. By comparing the evolution of the geometric structures and electronic properties before and after adsorption, we analyzed the regulation mechanisms of co-doping on gas adsorption at the atomic scale. Fig. 1a shows the stable structures of the structurally optimized MoS_2 monolayer and the three gas molecules. Bond length analysis indicated that all three molecules maintained typical symmetric structures, with bond lengths of 0.75, 1.14, and 0.98 Å for the H-H, C-O, and O-H bonds, respectively. These values agree well with the experimentally reported data in the literature [37–40], fully validating the accuracy of our computational methods.

Fig. 1b shows the atomic structures and electronic properties of metal and nonmetal-codoped MoS_2 monolayer materials (Sc@B-MoS_2, Sc@N-MoS_2, Ti@B-MoS_2, and Ti@N-MoS_2). Structural characterization revealed that all modified systems exhibited only minor deformation and no atomic agglomeration, confirming the structural stability of the co-doping strategy. The charge density quantitatively characterizes the charge transfer between different atoms [41–43], with the blue regions in Fig. 1b representing electron-rich zones and the red regions representing electron-depleted zones. The calculation results indicate that Sc/Ti metal atoms act as electron donors, forming significant electron-depleted regions around their doping sites, whereas B/N non-metal atoms act as electron acceptors, inducing distinct electron-enriched regions around them (specific data are shown in Table S1). This differentiated charge distribution directly reflects the

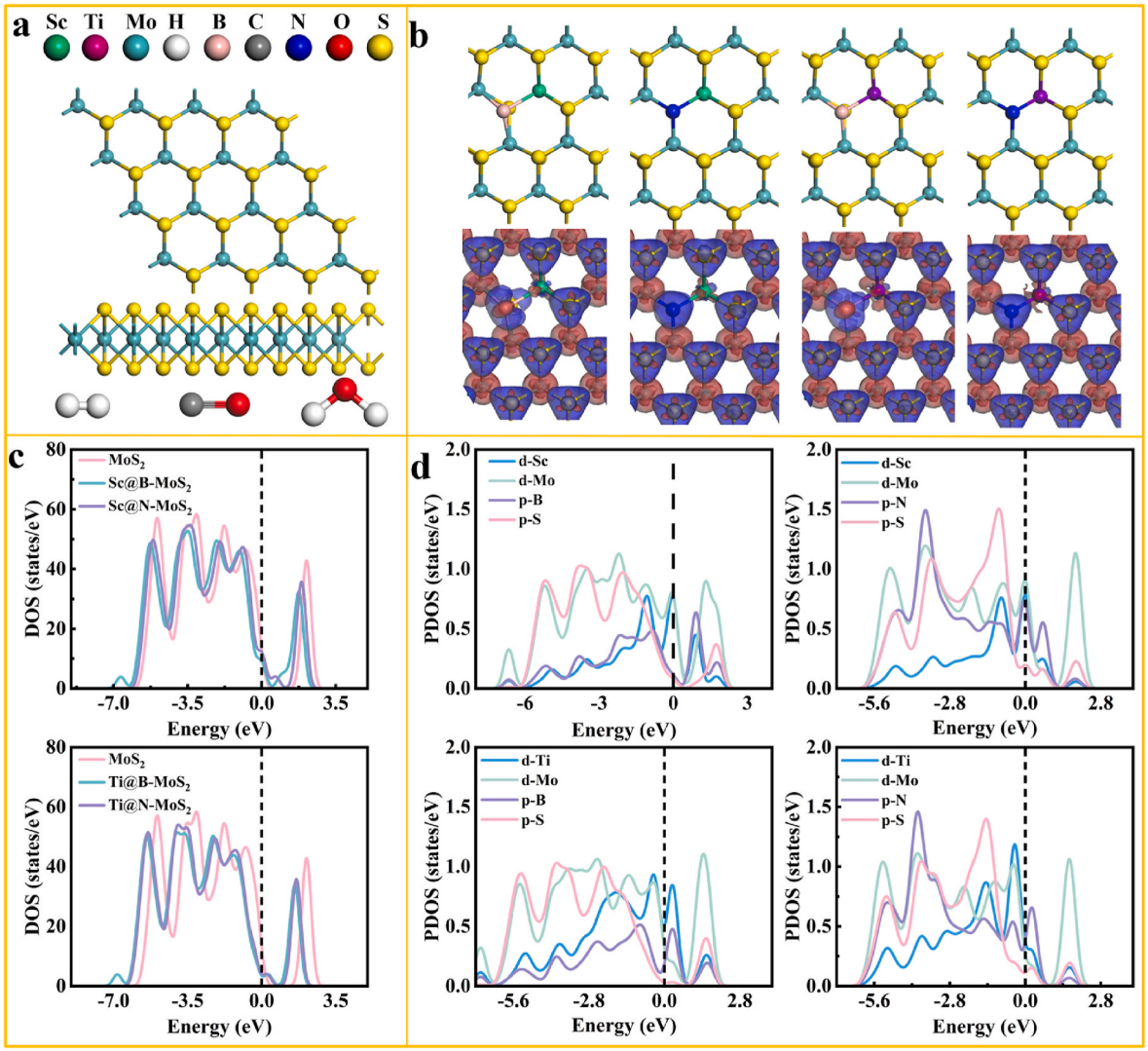

Fig. 1. (a) Schematic of the structural model for MoS_2 single-layer material and gas molecules (H_2, CO, and H_2O). (b) Stable structures and charge density maps of Sc@B-MoS_2, Sc@N-MoS_2, Ti@B-MoS_2, and Ti@N-MoS_2. (c) The density of states (DOS) and (d) projected density of states (PDOS) analysis plots for Sc@B-MoS_2, Sc@N-MoS_2, Ti@B-MoS_2, and Ti@N-MoS_2.

electronic interaction mechanism between the doped atoms and MoS_2 substrate. This not only effectively regulates the surface electron density, but more importantly, forms active sites with Lewis's acid-base characteristics at the Sc/Ti-B/N active centers, creating a favorable electronic environment for the subsequent selective adsorption and activation of gas molecules.

Moreover, the binding ability of metal and non-metal doping atoms to the surface was quantitatively characterized using formation energy and DOS diagrams [44]. First, the formation energy (E_f) [45–47] was analyzed as follows:

$$E_f = E_{TM@NTM\text{-}MoS_2} - E_{MoS_2} - n\mu_{TM} - m\mu_{NTM} + x\mu_s + y\mu_{Mo} \quad (1)$$

$E_{TM@NTM\text{-}MoS_2}$ and E_{MoS_2} denote the total energies of doped and undoped MoS_2, respectively. where μ_{TM} and μ_{NTM} represent the chemical potentials of the metal and nonmetal atoms, respectively. Here, μ_s and μ_{Mo} denote the chemical potentials of the S and Mo atoms. where m and n denote the number of metal and nonmetal atoms doped into the supercell. where x represents the number of S atoms replaced by the doped atoms and y represents the number of Mo atoms replaced by the doped atoms. A more negative E_f indicates greater stability of the doped system. The negative formation energies obtained for all the co-doped systems (Sc@B-MoS_2: 3.08 eV, Sc@N-MoS_2: 3.34 eV, Ti@B-MoS_2: 3.01 eV, Ti@N-MoS_2: 3.21 eV) indicate thermodynamic feasibility and a tendency. The well-preserved lattice structure after doping further supports this conclusion, as no significant distortion was observed, thus confirming the structural stability of these configurations.

For advanced gas sensor development, precise control of the electronic properties and active sites on material surfaces is key to achieving high-performance sensing. The work function, a key parameter characterizing the electronic escape properties of materials, directly reflects the work needed to extract an electron across the material-vacuum interface [48–51]. This study obtained the work function values of different modification systems through systematic calculations: the work functions of Sc@B-MoS_2, Sc@N-MoS_2, Ti@B-MoS_2, and Ti@N--MoS_2 were 5.80, 5.93, 5.85, and 6.07 eV, respectively. Computational analysis reveals that the work functions of Sc@B-MoS_2 and Ti@B-MoS_2 are lower than those of Sc@N-MoS_2 and Ti@N-MoS_2, respectively. The charge density analysis (Fig. 1b) indicates that the strong electronegativity of the nitrogen centers in the N-functionalized structures leads to a significant electron aggregation effect, whereas the electron loss of the metal atoms is insufficient to offset this process, leading to a decrease in the net electron concentration at the material surface and a significant increase in the work function of the material.

Further analysis of the surface electrostatic potential (Fig. S1) revealed that metal doping sites form localized high electrostatic potential regions, which promote gas adsorption through strong polarization effects and d-orbital hybridization. Meanwhile, the N atom regions enhance the activity of the metal sites through electron-induced effects and stabilize the adsorption products through charge complementarity. This “high-low” synergistic distribution pattern of the electrostatic potential enables the doped MoS_2 surface to form highly efficient gas adsorption active centers.

Under the B modification system, although B also exhibits electronic induction effects, its electronegativity is lower than that of N and Mo, resulting in a weaker electron-binding capacity. Additionally, the electrons lost by the metal atoms are not fully captured by B, leading to B sites retaining weak electron deficiency characteristics. Together with the metal sites, this forms an overall high electrostatic potential region. Notably, the Ti@N-MoS_2 system exhibits the highest work function value (6.61 eV), which is directly related to its charge transfer quantity (Ti: 0.53 e^-; N: 0.62 e^-), indicating that by precisely controlling the electron donation and acceptance capabilities of the dopant elements, the electronic properties of the material surface can be selectively optimized, thereby enhancing the adsorption capacity for specific gases.

Previous researches [52,53] have demonstrated that changes in the density of states directly affect the electrical response of a material, which is critical to gas-sensing performance. This study reveals the influence of atomic doping on the electrical response of materials by systematically analyzing the changes in the density of states curve. As shown in Fig. 1c, compared to pristine MoS_2, the density of states in all doped systems (Sc@B-MoS_2, Sc@N-MoS_2, Ti@B-MoS_2, and Ti@N-MoS_2) exhibited a significant shift toward lower energy levels, promoting interband electron transitions and indicating an enhanced electrical response. Specifically, compared to Sc@B-MoS_2 and Ti@B-MoS_2, Sc@N-MoS_2 and Ti@N-MoS_2 exhibited pronounced changes near the Fermi level. The new peaks observed near the Fermi level in the Sc-doped system indicate the emergence of novel electronic states. Upon H_2 molecule adsorption, these states can serve as efficient charge-transfer pathways, facilitating electron exchange between the adsorbate and substrate. Concurrently, alterations in the electronic structure, including the emergence of new peaks and band shifts, are expected to modulate the intrinsic carrier concentration and type of material. Such adjustments may induce corresponding changes in the electrical response, which typically create favorable conditions for inducing observable electrical responses during subsequent gas adsorption processes.

To further investigate the microscopic mechanisms of synergistic doping between metal and non-metal atoms, we calculated the PDOS for each system [54]. Fig. 1d illustrates the orbital interaction characteristics of the different co-doped MoS_2 systems. Calculations reveal that across all modified systems, the d orbitals of metal atoms (Mo/Sc/Ti) and p orbitals of non-metal atoms (S/B/N) show substantial orbital overlap, validating the stability of the doped structure. Notably, the N-doped systems (Sc@N-MoS_2 and Ti@N-MoS_2) exhibited stronger orbital hybridization characteristics than the B-doped systems. Specifically, within the energy range near the Fermi level (−3 to 0 eV), the projected density of states (PDOS) peaks of the d orbitals from Sc/Ti/Mo and the p orbitals from S/N exhibited more pronounced overlap and resonance, with the overall hybridization peaks exhibiting higher intensity. These features collectively indicate that in the N-co-modified systems, the electronic interactions between the atomic orbitals are more active and the orbital coupling is stronger.

3.2. Gas-Sc/Ti-B/N-MoS_2 surface

3.2.1. Gas-surface interaction mechanism

Employing a systematic methodology, this investigation explored the adsorption characteristics of gas in different co-doped MoS_2 systems using a multi-scale approach. First, the interaction strength of the different systems was determined through adsorption energy and distance analysis. Subsequently, the microscopic mechanism underlying the differences in adsorption performance was revealed by combining the transition metal d-state theory and COHP. To methodically investigate the adsorption behaviors of gas molecules on the surface of Sc/Ti-B/N-MoS_2 materials, we first constructed initial adsorption models for H_2, CO, and H_2O molecules at a distance of 2.50 Å above the monolayer material [37–40]. The equilibrium positions of each gas molecule were determined through structural optimization calculations (Fig. S2–S13). The most favorable adsorption geometry was identified through a comprehensive analysis of the relative energetic stabilities of various possible adsorption sites and molecular orientations (Fig. S14–S17).

Figs. 2 and 3 illustrate the optimal adsorption configurations of H_2, CO, and H_2O on Sc/Ti-B/N-MoS_2, with significant differences in the gas adsorption selectivity among the different doping systems. The distance between the adsorbate and substrate is an essential parameter for measuring bond strength. DFT calculations show that there are significant differences in the adsorption distances between the Sc@B-MoS_2 surface and different gas molecules: H_2O (2.35 Å) > H_2 (2.23 Å) > CO (2.13 Å). This distance gradient clearly reflects the material's selective adsorption properties toward gas molecules. The adsorption distances of Sc@N-MoS_2 for different gases showed gradient changes: H_2 (2.12 Å) <

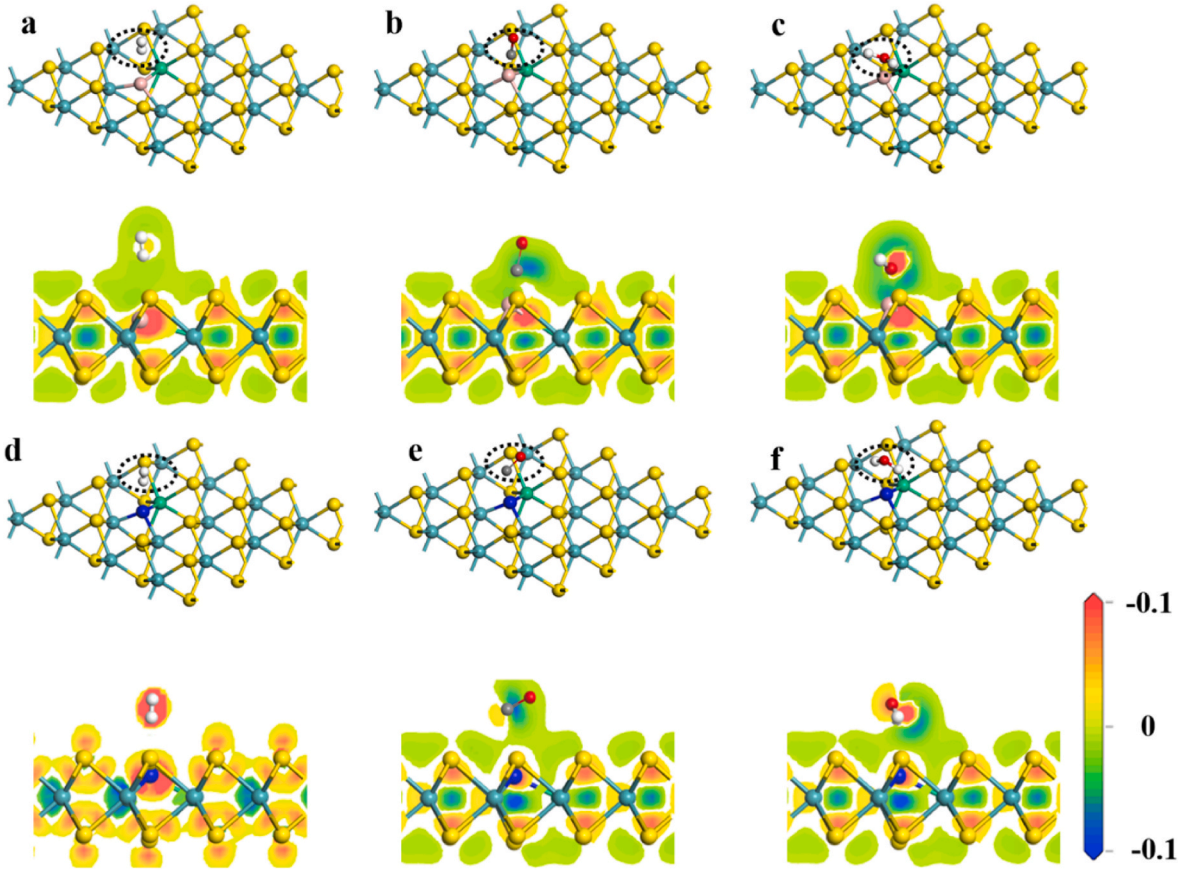

Fig. 2. Equilibrium adsorption geometries and electronic density profiles of different gas molecules on the surfaces of Sc@B-MoS_2 and Sc@N-MoS_2 materials: (a) Sc@B-MoS_2-H_2, (b) Sc@B-MoS_2-CO, (c) Sc@B-MoS_2-H_2O, (d) Sc@N-MoS_2-H_2, (e) Sc@N-MoS_2-CO, and (f) Sc@N-MoS_2-H_2O.

CO (2.24 Å) < H_2O (2.25 Å). The Ti-doped system shows more significant differences: the adsorption distances of Ti@B-MoS_2 for H_2, CO and H_2O are 2.28 Å, 2.12 Å and 2.29 Å, respectively. The corresponding values of Ti@N-MoS_2 are 2.22 Å, 2.25 Å and 2.18 Å respectively. All gas molecules in the optimized system underwent positional adjustments.

To elucidate the electronic interaction mechanism between gas molecules and functionalized MoS_2 surfaces, this study analyzed the charge distribution of the system using electron density [55] (Figs. 2 and 3). The electronic wave functions indicate that when gas molecules adsorb onto various material surfaces, they act as electron donors, transferring electrons to materials such as Sc@B-MoS_2, Sc@N-MoS_2, Ti@B-MoS_2, and Ti@N-MoS_2. This is consistent with the distribution characteristics shown in the red regions of the figure, indicating strong interactions between the gas and different surfaces.

To further validate the superiority of the synergistic effect in the co-doped system, we systematically calculated the charge transfer values (Table S2) and adsorption distances (Table S3) for the single-atom-doped system. The analysis shows that the co-doped system promotes stronger interfacial charge redistribution and smaller adsorption distances, providing direct evidence of its synergistic mechanism. To understand the interaction mechanism between the adsorbate (H_2, CO, H_2O) and Sc/Ti-B/N-MoS_2 system, we first conducted a theoretical analysis of the key parameters governing the adsorption characteristics. This study revealed a clear structure-property relationship between the adsorption distance and adsorption energy. As the adsorption distance decreased, the interfacial charge transfer effect intensified, leading to more negative adsorption energy values, indicating the formation of a more stable adsorption configuration [56]. Notably, the stable adsorption achieved by the co-doped system operates within an "effective response range" enhancing the recognition sensitivity for target gases, through strengthened interactions while maintaining adsorption-desorption reversibility. This demonstrates the core value of synergistic effects in optimizing the sensor performance. Based on this theoretical understanding, this work systematically compared the adsorption energies and distances of H_2, CO, and H_2O for four modified systems: Sc@B-MoS_2, Sc@N-MoS_2, Ti@B-MoS_2, and Ti@N-MoS_2. The adsorption energy calculation formula [57–59]:

$$E_{ads} = E_{total} - \left(E_{\text{monolayer}} + E_{gas}\right) \quad (2)$$

E_{ads} denotes the adsorption energy (eV), E_{total} reflects the stabilized energy minimum post gas adsorption, E_{gas} characterizes the ground-state energy of isolated gas molecules, and $E_{monolayer}$ represents the total energy of the ground state of intrinsic monolayer materials. As shown in Fig. 4a, the adsorption distance analysis revealed that the adsorption distances for all systems toward the three gases exceeded the sum of their respective atomic radii, indicating that physical adsorption predominated in all cases. On the Sc@B-MoS_2 surface, H_2 and CO molecules were adsorbed with moderate strength, exhibiting energies of −0.28 eV (2.23 Å) and −0.32 eV (2.13 Å), respectively. In contrast, H_2O binds more weakly, with an energy of −0.25 eV at a distance of 2.35 Å. For the Ti@N-MoS_2 system, the adsorption energies of H_2, CO, and H_2O were calculated to be −0.31 eV (2.22 Å), −0.27 eV (2.25 Å), and −0.22 eV (2.28 Å), respectively. This indicates that H_2 exhibits the strongest affinity on this surface, whereas H_2O is the most weakly adsorbed. In the case of Ti@B-MoS_2, CO exhibited the strongest adsorption among the three gases, with an energy of −0.34 eV at a close distance of 2.12 Å. The adsorption of H_2 (−0.26 eV, 2.28 Å) and H_2O (−0.19 eV, 2.29 Å) was significantly weaker. Finally, the adsorption on Sc@N-MoS_2 showed a distinct behavior: H_2 adsorption was the most favorable in this system, with an energy of −0.35 eV and a short distance of 2.12 Å. CO and H_2O

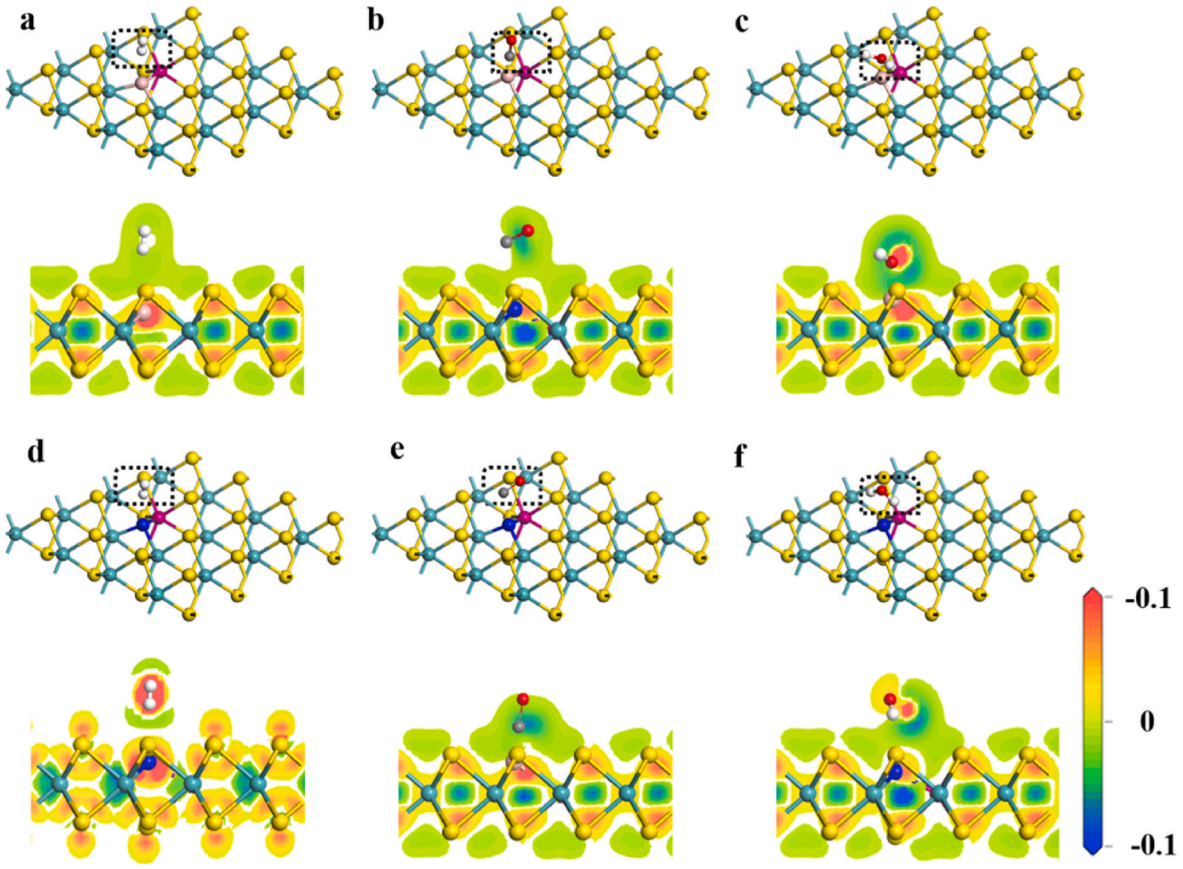

Fig. 3. Equilibrium adsorption geometries and electronic density profiles of different gas molecules on the surfaces of Ti@B-MoS_2 and Ti@N-MoS_2 materials: (a) Ti@B-MoS_2-H_2, (b) Ti@B-MoS_2-CO, (c) Ti@B-MoS_2-H_2O, (d) Ti@N-MoS_2-H_2, (e) Ti@N-MoS_2-CO, (f) Ti@N-MoS_2-H_2O.

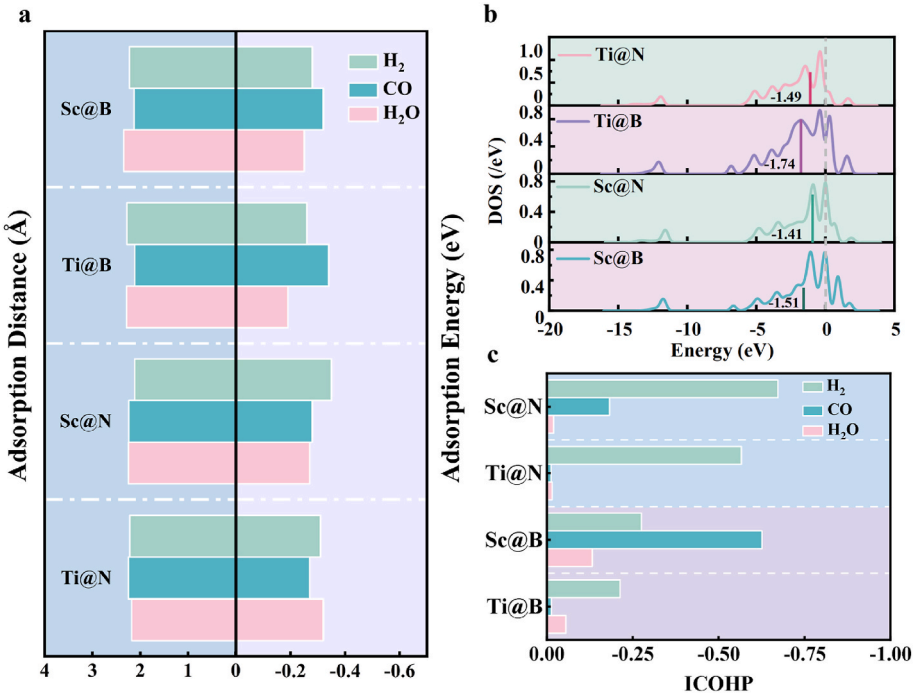

Fig. 4. (a) Adsorption energy and distance parameters of gas molecules (H_2, CO, and H_2O) on Sc@B-MoS_2, Ti@B-MoS_2, Sc@N-MoS_2, and Ti@N-MoS_2 materials, and (b) d-band centers of Sc@B-MoS_2, Ti@B-MoS_2, Sc@N-MoS_2, and Ti@N-MoS_2. (c) ICOHP of H_2, CO, and H_2O gas molecules on the surfaces of Sc@B-MoS_2, Ti@B-MoS_2, Sc@N-MoS_2, and Ti@N-MoS_2 materials.

are less strongly bound, with energies of −0.28 eV (2.24 Å) and −0.27 eV (2.25 Å), respectively. All calculated adsorption energies were

negative, ranging from −0.15 to −0.37 eV, confirming the exothermic and spontaneous nature of the adsorption processes. Additional adsorption energy data are presented in Table S4.

The d-band center theory is a key factor in evaluating the adsorption capabilities of metals. To elucidate the interaction mechanism between gas molecules and material surfaces, we calculated the d-band centers of different materials using the following specific calculation methods [60–62]:

$$\varepsilon_d = \frac{\int_{-\infty}^{\infty} n_d(\varepsilon)\varepsilon d\varepsilon}{\int_{-\infty}^{\infty} n_d(\varepsilon) d\varepsilon} \quad (3)$$

In this physical formula, ε represents energy, and $n_d(\varepsilon)$ represents density. Fig. 4b clearly illustrates the ε distribution characteristics of Sc/Ti-B/N-MoS_2. Interestingly, the value of ε and its position relative to the Fermi level significantly affect the material properties. As the value of ε increases and approaches the Fermi level, the electron coupling strengthens, and the gas adsorption becomes stronger. As shown in Fig. 4b, the ε values of the Sc@N-MoS_2 and Ti@N-MoS_2 systems are closer to the Fermi level than those of Sc@B-MoS_2 and Ti@B-MoS_2, indicating a stronger coupling between their d electronic states and gas molecular orbitals. This electronic structural characteristic directly leads to the superior performance of Sc@N-MoS_2 and Ti@N-MoS_2 in H_2 adsorption. Additionally, higher ε values increase the proportion of bonded states, thereby enhancing gas adsorption.

We then used chemical bond theory to thoroughly analyze the gas molecule adsorption mechanism on the surface of Sc/Ti-B/N-MoS_2 materials. We focused on the impact of electronic structure differences on the adsorption energy, with particular emphasis on the contribution of bonding orbitals to the adsorption stability. Building on previous research findings, this study employed the Crystal Orbital Hamilton Population method to quantitatively characterize the interatomic bonding interactions during the adsorption process, thereby revealing the essence of gas-surface interactions [63–65]. Fig. S18–21 present detailed COHP curves, which enable a precise analysis of the bonding and antibonding characteristics of chemical bonds and allow for a quantitative assessment of the bonding strength. The results indicate that the enhancement of bonding states below the Fermi level significantly increases the bonding cooperative force, whereas the weakening of antibonding states further reinforces this effect.

Fig. S19 and S21 show the COHP curves for Sc@N-MoS_2 and Ti@N-MoS_2 with respect to H_2, CO, and H_2O, respectively. As shown in the figures, CO and H_2O predominantly exhibit antibonding orbital interactions below the Fermi level when adsorbed on Sc@N-MoS_2 and Ti@N-MoS_2, leading to repulsive forces between atoms, weakened interatomic attraction, and unstable interactions. However, when H_2 adsorbs onto both materials, the interactions below the Fermi level are primarily dominated by the bonding orbitals. The filling of bonding orbital electrons enhances the interatomic attraction, driving the formation of stable adsorption between the gas and material surface. The antibonding orbitals did not significantly disrupt the adsorption stability, indicating that Sc@N-MoS_2 and Ti@N-MoS_2 exhibited excellent adsorption performance for H_2.

Notably, the COHP curves of different gas-material systems exhibited significant differences, reflecting the specificity of adsorption. We further calculated the integral COHP (ICOHP) values to provide a more quantitative explanation of the results [66]. Quantitative analysis shows (Fig. 4c) that the ICOHP values of Sc@N-MoS_2 and Ti@N-MoS_2 surfaces interacting with H_2 are significantly higher than those of CO and H_2O. This electronic structure feature directly confirms that H_2 molecules have a clear competitive adsorption advantage on the surface of this type of material.

3.2.2. Gas electrical response

Based on DFT calculations, the electrical response characteristics of gas adsorption processes in different co-doped MoS_2 systems were systematically analyzed (Fig. S22–S25). The electrical response, as a direct indicator of the strength of the material-gas interactions, clearly reflects the specific recognition ability of each modified system toward gases through its dynamic response behavior. Tao et al. [67,68] have demonstrated that comparing the height of the Fermi level on the density of states curves before and after gas adsorption can effectively characterize the evolution of the electrical response of the material. Based on the above analysis, we optimized this change and defined it as an electrical response value. A higher electrical response value indicates a better material response to the gas, enabling the intuitive identification of material systems with optimal selectivity for the target gas. we defined the following formula:

$$G_s = E_{f\text{-}g} / E_{f\text{-}s} \quad (4)$$

In this formula, G_s denotes the electrical response value. Owing to the different states of the material surface before and after gas adsorption, the density of states at the Fermi level (E_f) undergoes a significant change: $E_{f\text{-}s}$ prior to adsorption and $E_{f\text{-}g}$ after adsorption. This variation reflects the impact of gas adsorption on the distribution of electronic structures near the Fermi level of the material.

Fig. 5a shows the electrical response characteristics of the Sc@N-MoS_2 and Ti@N-MoS_2 monolayer materials toward H_2. As shown, both monolayer materials exhibited a significant selective response to H_2 gas in complex gas environments, accompanied by distinct electrical responses. Fig. 5b shows the electrical response of different monolayer materials to multiple gases. Sc@N-MoS_2 and Ti@N-MoS_2 exhibited highly selective electrical responses to H_2 in mixed-gas environments, whereas their responses to H_2O and CO were negligible. In contrast, although Sc@B-MoS_2 and Ti@B-MoS_2 also show high electrical response values for H_2, they simultaneously produce a significant electrical response to CO, indicating that the B-modified systems lack selective recognition capability. Notably, within the nitrogen-modified systems, Sc@N-MoS_2 exhibited superior H_2 electrical response characteristics compared to Ti@N-MoS_2, with more pronounced changes in the amplitude of the electrical signal. This further confirms the exceptional selective adsorption capability of the nitrogen-co-modified MoS_2 material for H_2.

To further investigate the gas adsorption characteristics, we systematically calculated the electronic structures of H_2, CO, and H_2O molecules on the surfaces of different co-doped MoS_2 systems (Fig. S22–S25). The results indicate that the B-modified systems (Sc@B-MoS_2 and Ti@B-MoS_2) cause a leftward shift in the energy bands and a slight decrease in the Fermi level when adsorbing CO and H_2, indicating a change in the electrical response; however, they lack a selective electrical response to H_2. In contrast, the N-modified systems (Sc@N-MoS_2 and Ti@N-MoS_2) exhibited significant electrical response selectivity, with the density of state curves remaining largely unchanged during the adsorption of CO and H_2O. The adsorption of H_2 resulted in a noticeable leftward shift in the band structure and a decrease in the Fermi level. Additionally, a new peak appeared near −3.6 eV for Ti@N-MoS_2 during H_2 adsorption, confirming a specific change in the electrical response. This unique response behavior not only verifies the selective recognition capability of N-modified materials toward H_2 but also highlights their excellent hydrophobic properties. Notably, the Sc@N-MoS_2 system exhibited superior performance to the Ti@N-MoS_2 system.

The selective adsorption mechanism of H_2 on the Sc@N-MoS_2 and Ti@N-MoS_2 surfaces was elucidated through a projected density of states (PDOS) analysis of the Sc/Ti-B/N-MoS_2 systems (Fig. S22–S25). The observed multiple hybridization peaks between −6.6 and −3.3 eV arise from the strong orbital overlap involving the H_2 s, metal (Sc/Ti) d, and N p orbitals. Notably, the characteristic peak at −3.6 eV in Ti@N-MoS_2 originates from the Ti 3d orbital contributions, whereas the broader density of states distribution near the Fermi level in Sc@N-MoS_2 accounts for its enhanced H_2 selectivity. These electronic structure

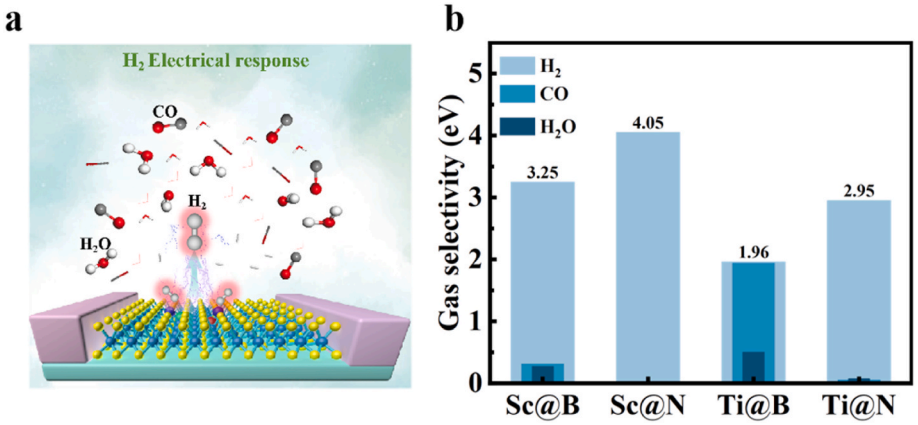

Fig. 5. (a) Co-doped MoS_2 monolayers: schematic of the H_2 response mechanism. (b) Comparison of the selectivity of modified Sc@B-MoS_2, Ti@B-MoS_2, Sc@N-MoS_2, and Ti@N-MoS_2 monolayers toward different gases.

features demonstrate the dominant role of the metal d orbitals in governing the adsorption selectivity and electrical response modulation of these materials.

3.3. Gas sensing applications

To investigate the performance of different co-doped MoS_2-based gas sensors for hydrogen detection, we focused on three key performance metrics: evaluating the material's temperature resistance through high-temperature stability testing, analyzing gas diffusion behavior and its impact on electrical response characteristics using molecular dynamics simulations, and quantitatively analyze dynamic parameters such as gas recovery time. These systematic studies provide comprehensive experimental evidence for understanding the performance of materials in actual working environments. Because the optimal operating temperature ranges vary among different materials, to ensure material performance and extend service life, we calculated the Gibbs free energies of H_2, CO, and H_2O on different surfaces to determine their optimal operating temperature ranges. The Gibbs free energy is expressed as follows:

$$G = E(OK) + H\text{-}T\cdot S \tag{5}$$

Where G is the Gibbs free energy and E(0 K) represents the total electronic energy of the system at absolute zero (this term incorporates the zero-point energy ZPE after frequency correction). H is the thermal correction to the enthalpy (integrated from the heat capacity) from 0 K to the target temperature T and S is the entropy, including translational, rotational, and vibrational contributions to the entropy. T is the absolute temperature. The specific calculation formula is provided in the Supporting Materials. The gas adsorption properties of the co-doped MoS_2 materials at different temperatures were evaluated using the Gibbs free energy (ΔG) system. ΔG was significantly positively correlated with

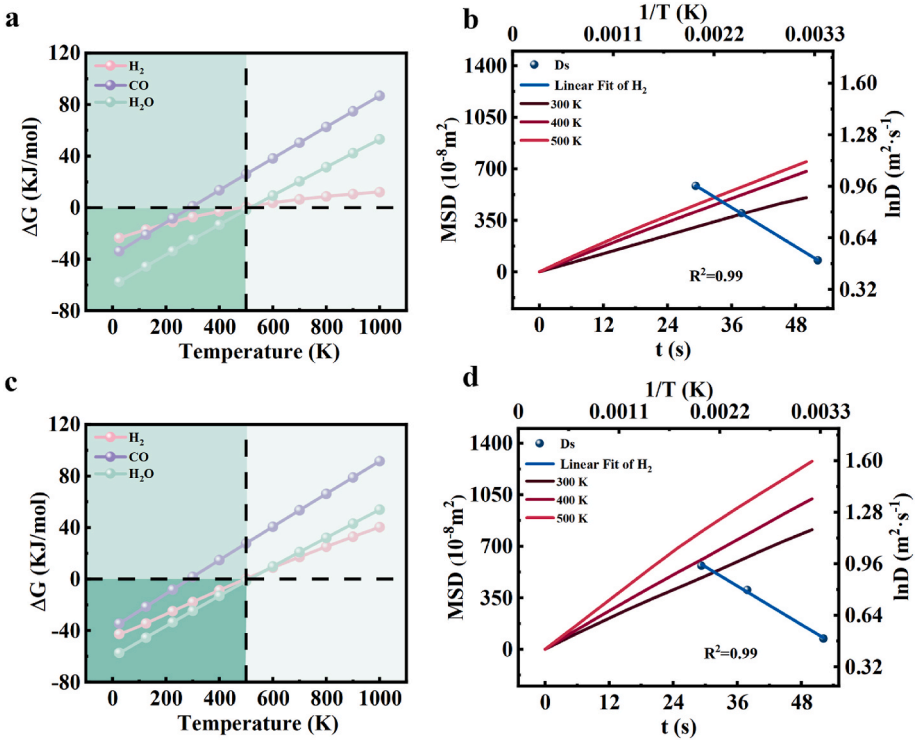

Fig. 6. Relationship between Gibbs free energy and temperature for three gases (H_2, CO, H_2O) on (a) Ti@N-MoS_2 and (c) Sc@N-MoS_2. Diffusion behavior of three gases at different temperatures in the (b) Ti@N-MoS_2 and (d) Sc@N-MoS_2 systems.

temperature, and the magnitude of the negative ΔG values corresponded to the strength of the adsorption capacity during spontaneous adsorption. As shown in Fig. 6a and c, at 275 K, the Sc@N-MoS_2 and Ti@N-MoS_2 systems exhibit $\Delta G > 0$ characteristics for CO, confirming that their effective adsorption capacity at room temperature does not possess stable adsorption characteristics at high temperatures. However, the selective adsorption of H_2 by Sc@N-MoS_2 and Ti@N-MoS_2 remained stable at elevated temperatures, with an operational temperature range far exceeding that of Sc@B-MoS_2 and Ti@B-MoS_2 (Fig. S34). This property stems from hydrogen exhibiting a larger negative free energy value when adsorbed onto Sc@N-MoS_2 and Ti@N-MoS_2 materials, enabling them to maintain superior adsorption performance under high-temperature conditions while demonstrating excellent stability against humidity fluctuations. This further validates the potential of these sensors for detecting hydrogen leaks in complex environments.

Molecular dynamics simulations were employed to characterize the diffusion properties of gas molecules on the co-doped MoS_2 surfaces. By calculating the diffusion coefficients at various temperatures and determining the activation energy for diffusion based on the Arrhenius equation, a comprehensive analysis of the gas diffusion kinetics was conducted (detailed computational methods are provided in the Supporting information). Research indicates that the diffusion coefficient is a physical parameter that characterizes the diffusion capability of molecules. A higher diffusion coefficient value corresponds to a faster molecular diffusion rate, indicating a lower energy barrier that must be overcome during the diffusion process. [69]. Fig. S26–S29 depict the initial and equilibrium configurations during gas adsorption, and the associated diffusion coefficients are summarized in Table S5 and S6**.** The Sc@N-MoS_2 and Ti@N-MoS_2 systems exhibit low diffusion coefficients for hydrogen gas but higher coefficients for CO and H_2O. This confirms, from a kinetic perspective, the selective adsorption capability of these materials toward H_2 molecules.

Fig. S30–S33 show the steady state of Sc/Ti-B/N-MoS_2-H_2 at different temperatures. Fig. 6b and d shows the equidistant displacement of H_2 on the modified Sc/Ti-N-MoS_2 electrode. The diffusion activation energy for H_2 was obtained by fitting the Arrhenius equation using the diffusion coefficients. Calculations indicated that the diffusion activation energies for Sc@N-MoS_2 and Ti@N-MoS_2 (−3.46 and - 3.86 kJ mol^{-1}, respectively) were significantly lower than those for Sc@B-MoS_2 and Ti@B-MoS_2 (−4.76 and - 3.92 kJ mol^{-1}, respectively), further confirming the superior performance of Sc@N-MoS_2 and Ti@N-MoS_2 in H_2 detection. In gas sensor performance evaluation, a preferable short recovery time (τ) serves as a core performance parameter that quantitatively describes the time required for the device to recover from exposure to the target gas to 90 % of its initial resistance value. This parameter is calculated using the following formula [70]:

$$\tau = A^{-1} e^{-E_{ads}/kT} \tag{6}$$

The parameters involved in the calculation include the temperature T, Boltzmann constant k, specified sampling frequency n, and prefactor A (taken as here 1×10^{13} s^{-1}). Physically, A represents the average number of attempts per second by the adsorbed molecules to overcome the surface potential barrier. The typical value (1×10^{13} s^{-1}) corresponds to the characteristic vibrational frequency of the surface chemical bonds. This value provides a reasonable benchmark for accurately assessing the hydrogen desorption energy barriers and related kinetic processes [71–73]. Table 1 lists the recovery time (τ) of the main co-doped system (Sc@N-MoS_2) in the relevant temperature range. Preferable short recovery time values correspond to smaller desorption energy barriers, indicating that the material possesses rapid desorption and efficient surface regeneration capabilities [74]. Table S7–S9 summarize the recovery time data for Sc/Ti-B/N-MoS_2 for multiple gases at different temperatures. The analysis revealed that the Sc@N-MoS_2 and Ti@N-MoS_2 monolayer materials exhibited superior desorption kinetics. With increasing temperature, the recovery time generally decreased, reflecting accelerated gas desorption rates [75]. Compared with Sc@B-MoS_2 and Ti@B-MoS_2, Sc@N-MoS_2 and Ti@N-MoS_2 exhibited a preferable short recovery time under most conditions, demonstrating their ideal short recovery characteristics as sensing materials, which is a critical property for real-time cyclic detection. Notably, hydrogen exhibits relatively longer τ values owing to its stronger adsorption, consistent with previous experimental observations. Nevertheless, Sc@N-MoS_2 and Ti@N-MoS_2 maintained high electrical responsivity toward H_2, even at elevated temperatures. This indicates that they preserve selectivity without sacrificing the recovery speed, demonstrating their significant potential for dynamic sensing applications.

Table 1
The recovery time (10^{-10} s) of the gas doped on the Sc@N-MoS_2.

T (K)	H_2	CO	H_2O
273	2880.00	1500.00	96.00
300	755.00	50.00	34.00
400	25.60	3.40	2.50
500	3.36	0.66	0.53

4. Conclusion

Employing density functional theory, this work systematically examined the differential adsorption behaviors of H_2, CO, and H_2O on Sc/Ti-B/N co-doped MoS_2, revealing a synergistic interaction mechanism between the metal and non-metal atoms. DFT calculations corroborated that the synergistic modification of metal (Sc/Ti) and non-metal (N) atoms markedly improved the material's H_2 adsorption selectivity. Specifically, Sc and Ti act as electron donors, transferring 0.74 and 0.53 electrons to the substrate, respectively, to form highly active sites with unoccupied d-orbitals. Their 3d orbitals undergo strong hybridization with the s orbitals of H_2, significantly enhancing the strength of the adsorption. N atoms, with their high electronegativity, capture 0.62–0.67 electrons to form a stable p-d hybridization network. The Sc-N synergistic combination exhibited the most outstanding performance. The 3d orbitals of Sc and the 2p orbitals of N form new hybridization peaks near the Fermi level. The adsorption energy of H_2 was −0.35 eV (ensuring high sensitivity) while maintaining an extremely low diffusion activation energy (only 3.46 kJ/mol). This achieves an ideal balance between strong adsorption and fast surface migration dynamics, providing a key theoretical basis for designing sensors that combine a preferable short recovery time with a higher electrical response. Density of states analysis and molecular dynamics simulations further confirmed that this modified system maintained excellent H_2 adsorption performance (diffusion coefficient 1.64×10^{-8} m^2/s to 2.58×10^{-8} m^2/s) and good hydrophobic properties (diffusion coefficient 5.41×10^{-8} m^2/s to 0.56×10^{-7} m^2/s) across a wide temperature range of 300–500 K. The pronounced electrical response values and preferable short recovery time demonstrate that the synergistic modification of MoS_2 with Sc/N and Ti/N achieves an optimal balance between high H_2 selectivity, significant electrical response, and short recovery time. This study elucidates the electronic structure mechanism by which metal-nonmetal synergistic modification enhances H_2 adsorption and overcomes the performance limitations of traditional single-atom-modified materials, providing important theoretical guidance and design strategies for developing novel high-performance hydrogen sensors.

CRediT authorship contribution statement

Zuxun Zhang: Writing – original draft, Methodology, Investigation, Formal analysis, Data curation. **Lin Tao:** Writing – review & editing, Validation, Supervision, Methodology, Funding acquisition, Conceptualization. **Xin Quan:** Methodology, Formal analysis. **Mingyang Gu:** Methodology, Formal analysis. **Han Zhang:** Methodology, Formal analysis, Data curation. **Baigang An:** Supervision, Formal analysis. **Lixiang Li:** Writing – review & editing, Supervision, Resources,

Methodology.

Declaration of competing interest

The authors declare that they have no known competing financial interests or personal relationships that could have appeared to influence the work reported in this paper.

Acknowledgment

The funding from the National Natural Science Foundation of China (Grant No. 52304330), the Natural Science Foundation of Liaoning Province (Grant No. 2024-BS-218), University of Science and Technology Liaoning Talent Project Grants (Grant No. 6003000317), the Outstanding Youth Fund of University of Science and Technology Liaoning (Grant No. 2023YQ11), and the Youth Fund of the Education Department of Liaoning Province (Grant No. LJKQZ20222324) are gratefully acknowledged.

Appendix A. Supplementary data

Supplementary data to this article can be found online at https://doi.org/10.1016/j.mssp.2026.110460.

Data availability

Data will be made available on request.

References

[1] N. Johnson, M. Liebreich, D.M. Kammen, P. Ekins, R. McKenna, I. Staffell, Realistic roles for hydrogen in the future energy transition, Nat. Rev. Clean Technol. 1 (2025) 351–371.
[2] M. Sandstad, S. Krishnan, G. Myhre, M. Sand, R. Bieltvedt Skeie, What to consider when considering climate effects of hydrogen – towards an assessment framework, Int. J. Hydrogen Energy 145 (2025) 795–802.
[3] P. Phogat, B. Chand, Shreya, R. Jha, S. Singh, Hydrogen and methanol fuel cells: a comprehensive analysis of challenges, advances, and future prospects in clean energy, Int. J. Hydrogen Energy 109 (2025) 465–485.
[4] B.G. Pollet, I. Staffell, J.L. Shang, Current status of hybrid, battery and fuel cell electric vehicles: from electrochemistry to market prospects, Electrochim. Acta 84 (2012) 235–249.
[5] B.B. Choi, C.H. Hong, S.Y. Jeon, Monitoring LOHC hydrogenation status using surface plasmon resonance sensor, Int. J. Hydrogen Energy 150 (2025) 150167.
[6] T. Hübert, L. Boon-Brett, G. Black, U. Banach, Hydrogen sensors – a review, Sensor. Actuator. B Chem. 157 (2011) 329–352.
[7] Y. Luo, C. Zhang, B. Zheng, X. Geng, M. Debliquy, Hydrogen sensors based on noble metal doped metal-oxide semiconductor: a review, Int. J. Hydrogen Energy 42 (2017) 20386–20397.
[8] J. Zhou, C. Wang, X. Zhang, L. Jiang, R. Wu, Advances in two-dimensional layered materials for gas sensing, Mater. Sci. Eng. R Rep. 161 (2024) 100872.
[9] S. Ghosh, C.-J. Yang, J.-Y. Lai, Optically active two-dimensional MoS_2-based nanohybrids for various biosensing applications: a comprehensive review, Biosens. Bioelectron. 246 (2024) 115861.
[10] S. Rawat, P. Bamola, S. Chandel, H. Kala, C. Dwivedi, H. Sharma, Environmental gas sensing studies using flower-like MoS_2 hybrid structure, Mater. Today Proc. 83 (2023) 39–42.
[11] Q. Yue, Z. Shao, S. Chang, J. Li, Adsorption of gas molecules on monolayer MoS_2 and effect of applied electric field, Nanoscale Res. Lett. 8 (2013) 425.
[12] T. Kim, T.H. Lee, S.Y. Park, T.H. Eom, I. Cho, Y. Kim, C. Kim, S.A. Lee, M.-J. Choi, J.M. Suh, I.-S. Hwang, D. Lee, I. Park, H.W. Jang, Drastic gas sensing selectivity in 2-Dimensional MoS_2 nanoflakes by noble metal decoration, ACS Nano 17 (2023) 4404–4413.
[13] H. Liu, Z. Tan, Y. Niu, S. Wang, Y. Wang, Ir-decorated MoS_2 monolayer as a promising candidate to detect dissolved gas in transformer oil: a DFT study, Chem. Phys. Lett. 818 (2023) 140410.
[14] D. Zhu, J. Sun, S. Shu, Q. Chen, X. Feng, S. Zhang, Y. Li, S. Ou, P.J.L. Wu, Co-and V-Doped MoS_2 Nanosheet Composites for Efficient Hydrogen Evolution Reaction in the Universal pH Range, 2025.
[15] H. Liu, S. Yang, G. Lei, M. Xu, H. Xu, Z. Lan, Z. Wang, J. Xiong, H. Gu, Y-decorated MoS_2 monolayer for promising hydrogen storage: a DFT study, Int. J. Hydrogen Energy 47 (2022) 12096–12106.
[16] S. Yang, X. Wang, G. Lei, H. Xu, Z. Wang, J. Xiong, H. Gu, A DFT study on the outstanding hydrogen storage performance of the Ti-decorated MoS_2 monolayer, Surf. Interfaces 26 (2021) 101329.
[17] S. Yang, Y. Liu, G. Lei, Y. Xie, L. Peng, H. Xu, Z. Wang, H. Gu, A DFT study on the hydrogen storage performance of MoS_2 monolayers doped with group 8B transition metals, Int. J. Hydrogen Energy 46 (2021) 24233–24246.
[18] P. Ding, T. Wang, P. Chang, L. Guan, Z. Liu, C. Xu, J.J.A.A.M. Tao, Interfaces, multiple-strategy Design of MOF-derived N, P co-doped MoS_2 Electrocatalysts Toward Efficient Alkaline Hydrogen Evolution and Overall Water Splitting, 15, 2023, pp. 52506–52518.
[19] Z. Zhang, Y. Zhu, X. Shi, B. Qi, Y. Ding, Y. Du, W. Shi, J. Zhang, J. Liu, Y.J.A.F. M. Sang, Orbital-Morphology-Based Oxygen Reduction in a Correlated Oxide, 34, 2024 2316448.
[20] M.L. Weber, D. Jennings, S. Fearn, A. Cavallaro, M. Prochazka, A. Gutsche, L. Heymann, J. Guo, L. Yasin, S.J. Cooper, J. Mayer, W. Rheinheimer, R. Dittmann, R. Waser, O. Guillon, C. Lenser, S.J. Skinner, A. Aguadero, S. Nemšák, F. Gunkel, Thermal stability and coalescence dynamics of exsolved metal nanoparticles at charged perovskite surfaces, Nat. Commun. 15 (2024).
[21] J. Cao, J. Zhou, Y. Zhang, X. Liu, Theoretical study of H_2 adsorbed on monolayer MoS_2 doped with N, Si, P, Microelectron. Eng. 190 (2018) 63–67.
[22] S. Wu, H. Liu, M. Qu, A. Du, J. Fan, Q. Sun, B/C-doped MoS_2 as promising materials for nitrogen removal from natural gas: a first-principles computational study, Comput. Mater. Sci. 214 (2022) 111735.
[23] L. Wang, Y. Hu, J. Xu, Z. Huang, H. Lao, X. Xu, J. Xu, H. Tang, R. Yuan, Z. Wang, Dual non-metal atom doping enabled 2D 1T-MoS_2 cocatalyst with abundant edge-S active sites for efficient photocatalytic H_2 evolution, Int. J. Hydrogen Energy 48 (2023) 16987–16999.
[24] M. Pramanik, B. Jana, A. Ghatak, K.J.M.C. Das, Physics, Improvement in Efficiency of MoS_2 Nanoflower Based Ethylene Gas Sensor on Transition Metal Doping: an Experimental and Theoretical Investigation, 314, 2024 128892.
[25] S.Y. Choi, Y. Kim, H.-S. Chung, A.R. Kim, J.-D. Kwon, J. Park, Y.L. Kim, S.-H. Kwon, M.G. Hahm, B.J.A.a.m. Cho, Interfaces, Effect of Nb Doping on Chemical Sensing Performance of two-dimensional Layered $MoSe_2$, 9, 2017, pp. 3817–3823.
[26] D. Burman, H. Raha, B. Manna, P. Pramanik, P.K.J.A.s. Guha, Substitutional Doping of MoS_2 for Superior gas-sensing Applications: a Proof of Concept, 6, 2021, pp. 3398–3408.
[27] Y. Linghu, C. Wu, Gas molecules on defective and nonmetal-doped MoS2 monolayers, J. Phys. Chem. 124 (2019) 1511–1522.
[28] T. Liu, C. Fang, B. Yu, Y. You, H. Niu, R. Zhou, J. Zhang, J.J.I.C.F. Xu, Vanadium-Doping in interlayer-expanded MoS_2 Nanosheets for the Efficient Electrocatalytic Hydrogen Evolution Reaction, 7, 2020, pp. 2497–2505.
[29] S. Nazeer, S.E. Hussain, J.J.M.T.C. Qi, Synergistic Doping and Sulfur Vacancy Engineering in 1T-MoS_2 to Influence the Performance of Hydrogen Evaluation Reaction, 41, 2024 110708.
[30] B. Delley, From molecules to solids with the DMol 3 approach, J. Chem. Phys. 113 (2000) 7756–7764.
[31] J.P. Perdew, Y. Wang, Accurate and simple analytic representation of the electron-gas correlation energy, Phys. Rev. B 45 (1992) 13244.
[32] J.P. Perdew, K. Burke, M. Ernzerhof, Generalized gradient approximation made simple, Phys. Rev. Lett. 77 (1996) 3865.
[33] S. Grimme, Semiempirical GGA-type density functional constructed with a long-range dispersion correction, J. Comput. Chem. 27 (2006) 1787–1799.
[34] K.M. Bal, E.C. Neyts, Modelling molecular adsorption on charged or polarized surfaces: a critical flaw in common approaches, Phys. Chem. Chem. Phys. 20 (2018) 8456–8459.
[35] R.S. Mulliken, Electronic population analysis on LCAO–MO molecular wave functions. I, J. Chem. Phys. 23 (1955) 1833–1840.
[36] C. Song, L. Tao, J. Dang, D. Dastan, W. Wang, X. Zhang, L. Li, B. An, Tuning NO_2 selectivity in $MoSe_2$ sensors via metal modification: Fermi-level electronic state control, Comput. Theor. Chem. 1250 (2025) 115296.
[37] H.-Z. Wu, S. Bandaru, J. Liu, L.-L. Li, Z. Wang, Adsorption of H_2O, H_2 , O_2 , CO, NO, and CO_2 on graphene/g-C_3N_4 nanocomposite investigated by density functional theory, Appl. Surf. Sci. 430 (2018) 125–136.
[38] T. He, H. Liu, J. Zhang, Y. Yang, Y. Hu, Y. Zhang, K. Hu, DFT study on the adsorption and sensing properties of dissolved gases (H_2, CO and CH_4) in transformer oil on PdO-doped In_2O_3 (1 1 0) surfaces, Chem. Phys. Lett. 832 (2023) 140865.
[39] H. Guo, L. Li, X. Wang, G. Yao, H. Yu, Z. Tian, B. Li, L. Chen, Theoretical investigation on the single transition-metal atom-decorated defective MoS_2 for electrocatalytic ammonia synthesis, ACS Appl. Mater. Interfaces 11 (2019) 36506–36514.
[40] Y. Linghu, C. Wu, Gas molecules on defective and nonmetal-doped MoS_2 monolayers, J. Phys. Chem. C 124 (2019) 1511–1522.
[41] X. Luo, Y. Zhang, X. Qi, Y. Wu, Y. Fan, D. Su, J. Wen, A. Mahmood Ali, F. Jing, H. Zhang, A DFT study: single transition metal atom doped MoS_2 as efficient electrocatalysts for the nitrogen reduction reaction, ACS Appl. Nano Mater. 8 (2025) 10695–10703.
[42] H. Cui, G. Zhang, X. Zhang, J. Tang, Rh-doped $MoSe_2$ as a toxic gas scavenger: a first-principles study, Nanoscale Adv. 1 (2019) 772–780.
[43] X.Y. Yu, Z.Q. Huang, T. Ban, Y.H. Xu, Z.W. Liu, C.R. Chang, Finding natural, dense, and stable frustrated lewis pairs on wurtzite crystal surfaces for small-molecule activation, Angew. Chem. Int. Ed. 63 (2024).
[44] M. Brown, L. Diaz, A. Aslan, M. Sanati, S. Portillo, E. Schamiloglu, R.P. Joshi, Carbon-oxygen surface formation enhances secondary electron yield in Cu, Ag and Au, Sci. Rep. 12 (2022).
[45] Y. Du, S. Zhao, H. Tang, Z. Ni, S. Xia, An active MoS_2 with Pt-doping and sulfur vacancy for strengthen CO_2 adsorption and fast capture: a DFT approach, Chem. Phys. Lett. 802 (2022).

[46] M.D. Esrafili, H. Janebi, P. Mousavian, Single Al atom anchored on defective MoS_2: an efficient catalytic site for reduction of greenhouse N_2O gas by CO or C_2H_4 molecules, Appl. Surf. Sci. 569 (2021).
[47] Y. Zhao, J. Tu, Y. Zhang, X. Hu, Y. Xu, L. He, Improved photocatalytic property of monolayer MoS_2 by B and F co-doping: first principles study, J. Catal. 382 (2020) 280–285.
[48] R. Guarino, F. Mo, Y. Ardesi, A. Gaiardo, M. Tonezzer, S. Guarino, G. Piccinini, Modelling electronic transport in monocrystalline metal oxide gas sensors: from the surface kinetics to the experimental response, Sensor. Actuator. B Chem. 373 (2022) 132646.
[49] S.L. Amith, K. Gurunathan, Active sites tailored rGO-PPy nanosheets with high crystalline tetragonal SnO_2 nanocrystals for ammonia e-sensitization at room temperature, J. Alloys Compd. 960 (2023) 170819.
[50] U.D. Patil, S. Mahakal, D.M. Nerkar, H. Noothalapati, S. Shinde, S.A. Waghmode, D. Amalnerkar, Nanoarchitectured heteroatom-doped graphene as an adsorbent for dyes and heavy metals: historical account, recent advancement and future prospects, Inorg. Chem. Commun. 180 (2025) 114879.
[51] J. Wu, A. Huang, H. Hu, X. Gao, Z. Chen, Construction and enhancement of built-in electric field for efficient oxygen evolution reaction, J. Colloid Interface Sci. 674 (2024) 677–685.
[52] L. Tao, D. Dastan, W. Wang, P. Poldorn, X. Meng, M. Wu, H. Zhao, H. Zhang, L. Li, B. An, Metal-decorated InN monolayer senses N_2 against CO_2, ACS Appl. Mater. Interfaces 15 (2023) 12534–12544.
[53] S. Nie, J. Li, L. Tao, Y. He, D. Dastan, X. Meng, P. Poldorn, X. Yin, Insights into selective mechanism of NiO-TiO_2 heterojunction to H_2 and CO, ACS Sens. 8 (2023) 4121–4131.
[54] B. Li, Q. Zhou, R. Peng, Y. Liao, W. Zeng, Adsorption of SF_6 decomposition gases (H_2S, SO_2, SOF_2 and SO_2F_2) on Sc-doped MoS_2 surface: a DFT study, Appl. Surf. Sci. 549 (2021) 149271.
[55] P. Li, R. Zhou, B. Liu, Y. Yuan, H. Cui, Z.-H. Pu, T. Wu, Adsorption of a $MoSe_2$-Based sensor for fluorocarbon gas decomposition products in gas-insulated switchgear: a first principles analysis, J. Phys. Chem. C 127 (2023) 11176–11185.
[56] K.L. Milton, L. Hargreaves, A. Shluger, Structure and dynamics of water confined at the SiO_2/WS_2 interface, J. Phys. Chem. C 129 (2025) 4261–4271.
[57] L. Tao, J. Huang, X. Yin, Q. Wang, Z. Li, G. Wang, B. Cui, Adsorption kinetics of CO_2 on a reconstructed calcite surface: an experiment-simulation collaborative method, Energy Fuel. 33 (2019) 8946–8953.
[58] Y. He, J. Li, L. Tao, S. Nie, T. Fang, X. Yin, Q. Wang, First-principles calculations on the resistance and electronic properties of H_2 adsorption on a CoO–SnO_2 heterojunction surface, Phys. Chem. Chem. Phys. 24 (2022) 392–402.
[59] Y. He, L. Tao, J. Li, M. Wu, P. Poldorn, D. Dastan, S. Abbasi, S. Nie, X. Yin, Q. Wang, Atomic-level insights into selective adsorption of H_2 and CO on SnO_2/CoO heterojunctions, Mater. Today Nano 22 (2023) 100334.
[60] M. Wang, L. Kong, X. Lu, C.-M.L. Wu, First-row transition metal embedded pyrazine-based graphynes as high-performance single atom catalysts for the CO_2 reduction reaction, J. Mater. Chem. A 10 (2022) 9048–9058.
[61] M. Gu, L. Tao, D. Dastan, J. Dang, T. Fang, B. An, Metal-modified C_3N_1 monolayer sensors for battery instability monitoring, J. Mater. Chem. A 12 (2024) 15254–15264.
[62] L. Tao, Z. Li, G.-C. Wang, B.-Y. Cui, X.-T. Yin, Q. Wang, Evolution of calcite surface reconstruction and interface adsorption of calcite-CO_2 with temperature, Mater. Res. Express 6 (2018) 025035.
[63] Q. Wang, Y. Wang, Z. Li, X. Ma, DFT study on doping effect of different transition metals on MoS_2 for enhancing the formation of S vacancies, Int. J. Hydrogen Energy 82 (2024) 416–427.
[64] L. Nowakowski, F. Zasada, J. Gryboś, Z. Sojka, Orbital resolution of the reconstruction of CeO_2 (100) Facet–Hybrid-DFT and COHP investigations supported by HR-TEM imaging, J. Phys. Chem. C 129 (2025) 2165–2175.
[65] X. Guo, Q. Zhou, C. Wang, Y. Cao, X. Yang, S. Wei, W. Xu, S. Chen, K. Zhu, P. Zhang, H. Shou, Y. Wang, P.J. Chimtali, X. Wu, L. Song, X. Liu, Universal intercalation/alloying hybrid mechanism with -ICOHP criterion in MAX toward steadily ascending lithium-ion batteries, Small 20 (2024).
[66] N. Zhang, X. Chen, C. Sun, W. Xie, X. Wang, J. Yao, Revealing the key role of bonding states in surface chemisorption, Chem. Eng. Sci. 249 (2022) 117345.
[67] Y. Sun, L. Tao, M. Wu, D. Dastan, J. Rehman, L. Li, B. An, Multi-atomic loaded C_2N_1 catalysts for CO_2 reduction to CO or formic acid, Nanoscale 16 (2024) 9791–9801.
[68] M. Gu, L. Tao, D. Dastan, J. Dang, X. Zhang, L. Li, B. An, Metal-enhanced carbon-nitrogen material for selective detection of hazardous gases: insights from interface electronic states, Surf. Interfaces 53 (2024) 105097.
[69] L. Tao, J. Huang, D. Dastan, J. Li, X. Yin, Q. Wang, Flue gas separation at organic-inorganic interface under geological conditions, Surf. Interfaces 27 (2021) 101462.
[70] Y. Liu, L. Gao, S. Fu, S. Cheng, N. Gao, H. Li, Highly efficient VOC gas sensors based on Li-doped diamane, Appl. Surf. Sci. 611 (2023) 155694.
[71] C. Yu, F. Wang, Y. Zhang, L. Zhao, B. Teng, M. Fan, X. Liu, H_2 thermal desorption spectra on Pt(111): a density functional theory and kinetic Monte Carlo simulation study, Catalysts 8 (2018).
[72] M. Lototskyy, R. Denys, S. Nyallang Nyamsi, I. Bessarabskaia, V. Yartys, Modelling of hydrogen thermal desorption spectra, Mater. Today Proc. 5 (2018) 10440–10449.
[73] A. Gorski, V. Yurkiv, D. Starukhin, H.-R. Volpp, H_2O chemisorption and H_2 oxidation on yttria-stabilized zirconia: density functional theory and temperature-programmed desorption studies, J. Power Sources 196 (2011) 7188–7194.
[74] A. Agrawal, R. Kumar, S. Venkatesan, A. Zakhidov, Z. Zhu, J. Bao, M. Kumar, M. Kumar, Fast detection and low power hydrogen sensor using edge-oriented vertically aligned 3-D network of MoS_2 flakes at room temperature, Appl. Phys. Lett. 111 (2017).
[75] M. Lu, L. Tao, Y. Su, Y. Sun, D. Dastan, J. Rehman, H. Zhang, H. Zhao, L. Li, B. An, First-principles study of bonding-driven selectivity in CO_2 electroreduction on metal–nitrogen–carbon catalysts, J. Phys. Chem. C (2025), https://doi.org/10.1021/acs.jpcc.5c07261.